IEEE Access
Multidisciplinary ⋮ Rapid Review ⋮ Open Access Journal

Received January 5, 2022, accepted January 23, 2022, date of publication February 9, 2022, date of current version March 14, 2022.

Digital Object Identifier 10.1109/ACCESS.2022.3148970

Finite Difference Simulation of Fractal-Fractional Model of Electro-Osmotic Flow of Casson Fluid in a Micro Channel

SAQIB MURTAZA[1], POOM KUMAM[1,2,3], (Member, IEEE), ZUBAIR AHMAD[4], KANOKWAN SITTHITHAKERNGKIET[5], AND IBN E ALI[6]

[1]Department of Mathematics, Faculty of Science, King Mongkut's University of Technology Thonburi (KMUTT), Bang Mod, Thung Khru, Bangkok 10140, Thailand
[2]Center of Excellence in Theoretical and Computational Science (TaCS-CoE), Faculty of Science, King Mongkut's University of Technology Thonburi (KMUTT), Bang Mod, Thung Khru, Bangkok 10140, Thailand
[3]Department of Medical Research, China Medical University Hospital, China Medical University, Taichung 40402, Taiwan
[4]Dipartimento di Matematica e Fisica, Università degli Studi della Campania "Luigi Vanvitelli", 81100 Caserta, Italy
[5]Intelligent and Nonlinear Dynamic Innovations Research Center, Department of Mathematics, Faculty of Applied Science, King Mongkut's University of Technology North Bangkok (KMUTNB), Bangsue, Bangkok 10800, Thailand
[6]Higher Education Archives and Libraries Department KP, Government Superior Science College, Peshawar 25000, Pakistan

Corresponding author: Poom Kumam (poom.kum@kmutt.ac.th)

This work was supported in part by the Center of Excellence in Theoretical and Computational Science (TaCS-CoE), King Mongkut's University of Technology Thonburi, Thailand (KMUTT). Moreover, this research was funded by National Science, Research and Innovation Fund (NSRF), and King Mongkut's University of Technology North Bangkok with Contract no. KMUTNB-FF-65-24.

ABSTRACT In this work, an evolving definition of the fractal-fractional operator with exponential kernel was employed to examine Casson fluid flow with the electro-osmotic phenomenon. Electrically conducted Casson fluid flow with the effect of the electro-osmotic phenomenon has been assumed in a vertical microchannel. With the help of relative constitutive equations, the local mathematical model is formulated in terms of partially coupled partial differential equations along with appropriate physical initial and boundary conditions. The dimensional governing equations have been non-dimensional by using relative similarity variables to encounter the units and reduce the variables. The local mathematical model has been transformed to a fractal-fractional model by using a fractal-fractional derivative operator with exponential kernel and then analyze numerically with the discretization of finite difference (Crank-Nicolson) scheme. For an insight view of the proposed phenomena, various plots are drawn in respect of inserted parameter. From the graphical analysis, it has been observed that the electro-kinetic k parameter retards the fluid's motion. It is also worth noting that graphs for the fractal-fractional, fractional, and classical order parameters have been drawn. Due to the fractal order parameter, it was revealed that the fractal-fractional order model has a larger memory effect than the fractional-order and classical models.

INDEX TERMS Fractal-fractional model, finite difference scheme, electro-osmotic phenomenon, exponential memory kernel, zeta potential.

I. INTRODUCTION

Many real-world challenges are explained using fractional calculus (FC), which has a greater memory effect. FC is an extension of integer order calculus, which proved insufficient to explain some memory effects in some engineering and real-world issues. Because of its numerous uses in many disciplines of science, the FC is exhibiting a variety of phenomena that we refer to as memory. For various physical problems, many researchers established distinct definitions of fractional derivatives. In recent years, great progress has been made by employing fractional calculus [1]–[3], such as wave propagation [4], image processing [5], modeling of heart tissue [6], infectious disease [7]–[9], nanofluids [10]–[12], chemical kinetics [13] and electrical circuit analysis [14]. Researchers provided several fractional derivative operators over time, such as Riemann-Liouville [15], Caputo [16], and Caputo and Fabrizio [17], however many of these models were not applicable globally due to their local kernel. To address the difficulty raised in the previous models, Atangana and Baleanu [18] presented the Mittag-Leffler function in 2016 to make the kernel of the

The associate editor coordinating the review of this manuscript and approving it for publication was Lei Wang.

fractional derivative operator non-local. Murtaza *et al.* [19] examined the fractional electro-osmotic flow of Maxwell fluid together with upshots of joule heating. The authors analyzed the flow in a microchannel with the Mittage-Leffler kernel of the Atangana-Baleanu derivative. In another study, Murtaza *et al.* [20] found the exact solution of the non-linear mathematical model of Jeffery fluid. For the exact solution of the non-linear problem, the authors employed the fractional model of the Atangan-Baleanu derivative operator. Atangana [21] recently developed fractal-fractional derivatives in FC. This novel concept is well suited to a variety of complex physical phenomena. Fractal-fractional order derivative contains two orders in their operator: the first is known as the fractional-order, and the second is known as the fractal dimension. This new fractal fractional derivative idea outperforms both the classical and fractional derivatives. It is because working with fractal-fractional derivatives allows us to analyze both the fractional operator and the fractal dimension at the same time. Many scholars show their devotion and their interest in the fractal fractional operator because of its advanced and unique properties. Bearing in view the characteristics of the fractal-fractional operator, Arfan *et al*. [22] investigated the Covid-19 effects in Pakistan. Ali *et al.* [23] discussed the qualitative examinations of the Covid-19 mathematical model with the case study of Wuhan. Many other relative research works on the uses of the fractal-fractional operator can be found in [24]–[27].

Because of the broad spectrum of possible applications in pharmacological, biological, and biochemical fields, microscale transport dynamics is garnering significant interest [28]–[31]. Because of their capacity to construct millions of microchannels, cheap operating cost, ease of sample handling, and compactness, lab-on-chip (LOC) devices are widely used in the biomedical industry [32]–[34]. Electro-osmotic actuated flow is gaining popularity in the field of microfluidics due to its inherent advantages such as minimal moving components, low-pressure dips, and so on [34], [35]. The transport of electrolyte solutions with the formation of an electric double layer (EDL) consisting of the Stern layer and the diffuse or Guoy-Chapman layer next to charge substrates under the influence of an externally applied electric field is referred to as electro-osmotic flow [36], [37]. Over the years, researchers have been interested in the transport dynamics of electroosmotic flows with larger zeta potentials, i.e. (25–100 mV). The viscoelastic effect is considerable at higher zeta potentials and plays an important role in describing flow fields [38], [39]. In the light of the above-stated significances, Cao *et al.* [40] examined numerically the electro-osmotic flow of second grade fluid via the fractional operator in a rotating frame. Baños *et al.* [41] did mass transport analysis of concentration species via electro-osmotic phenomena in a slit microchannel. Some other interesting and note-worthy research work related to the electro-osmotic phenomena can be seen in [42]–[44].

The Casson fluid model is a shear-thinning non-Newtonian fluid model with yield stress. NonNewtonian fluids are commonly found in technical applications such as crude oil extraction, paint manufacture, and the food sector. Atlas *et al.* [45] recently studied the unsteady heat and mass transport of a Casson fluid with heat and mass flux boundary conditions. Shehzad *et al.* [46] investigated the influence of internal heat production and radiation on the flow of a Casson fluid in the presence of a magnetic field. Other recent studies on Casson fluids may be found in [47]–[52].

From a comprehensive analysis of the literature, no study has been reported related to the analysis of the electro-osmotic flow of Casson fluid via a fractal-fractional operator. Therefore, to fill this gap, an unsteady free convection flow of Casson fluid in a vertical micro channel together with the effect of the electroosmotic phenomenon has been assumed. In the present study, the authors generalized the classical model with the help of fractal-fractional operator of Caputo-Fabrizio with exponential kernel for analysis of the fluid's rheology. The numerical solution of the proposed problem has been found via the finite difference (Crank-Nicolson) approach. Graphical results are sketched for inserted non-dimensional parameters and illustrated logically.

II. FORMULATION OF THE PROBLEM

In the presence of electro-osmosis, an unsteady flow of Casson fluid in a vertical microchannel of length l has been assumed. The motion of the Casson fluid has been considered along the x-axis. The asymmetric zeta potential ξ_1 and ξ_2 is preserved by the channel plates and the fluid motion is exposed to the transverse magnetic field of magnitude B_0. Initially, both the plates of the microchannel and fluid have been considered stationary with surrounding temperature T_s and concentration C_s. For time ($\tau > 0$), the right plate ($y = l$) begins to move along its axis at a constant velocity $U_0H(\tau)$, and its temperature and concentration are raised to $T_s + (T_p - T_s)A\tau$ and $C_s + (C_p - C_s)A\tau$ respectively. The geometrical illustration of the problem is shown in Fig.1.

In the light of the following assumptions:

- ➢ Unsteady Flow
- ➢ Laminar Flow
- ➢ Incompressible Flow
- ➢ Electro-osmotic Effect
- ➢ Natural Convection
- ➢ Magnetic Field Effect
- ➢ Time Dependent Temperature
- ➢ Time Dependent Concentration
- ➢ Vertical Channel
- ➢ Ignoring Pressure Gradient

the velocity, thermal, concentration, electric and magnetic fields are given as:

$$\left.\begin{aligned} \overrightarrow{V} &= \{u(\zeta,\tau),0,0\} \\ \overrightarrow{T} &= \{T(\zeta,\tau),0,0\} \\ \overrightarrow{C} &= \{C(\zeta,\tau),0,0\} \\ \overrightarrow{E} &= \{E_x,0,0\} \\ \overrightarrow{B} &= \{0,B_0,0\} \end{aligned}\right], \tag{1}$$

The governing equations for the velocity field in the presence of electro-osmotic phenomena is stated as:

$$\rho \frac{d\overrightarrow{V}}{d\tau} = div\left(\boldsymbol{\tau}_{ij}\right) + \rho\overrightarrow{F}, \tag{2}$$

In Eq. (2), $\overrightarrow{V}$ and $\boldsymbol{\tau}_{ij}$ indicates the velocity and Cauchy stress tensor respectively, while $\rho\overrightarrow{F}$ showing body forces and addressed as:

$$\rho\overrightarrow{F} = \mathbf{J} \times \mathbf{B} + \rho\overrightarrow{g} + \overrightarrow{E}\,\rho_e. \tag{3}$$

In Eq.(3) $\mathbf{J} \times \mathbf{B}$ represents the drag (Lorentz) forces, ρ represent the effective density of the fluid, $\overrightarrow{g}$ represent gravitational acceleration, $\overrightarrow{E}$ represent the electric field and ρ_e represent the net charge density which governs by Poisson equation''

$$\nabla^2\psi = \frac{\rho_e}{\varepsilon} \tag{4}$$

where the net charge density for an electrolyte solution is given by Boltzmann distribution as:

$$\rho_e = 2n_0 e z_v \sinh\left(\frac{e z_v \psi}{k_B T_{av}}\right), \tag{5}$$

where z_v shows the valence, n_0 gives the ion density, e is the fundamental charge, k_B represents the Boltzmann constant and T_{av} is the absolute temperature.

From Debye-Huckel linearization approximation, we have:

$$\sinh\left(\frac{e z_v \psi}{k_B T_{av}}\right) \approx \frac{e z_v \psi}{k_B T_{av}}, \tag{6}$$

using equation (6) in (4), we get:

$$\frac{d^2\psi}{d\varsigma^2} = \frac{2n_0 e^2 z_v^2 \psi}{\varepsilon k_B T_{av}}. \tag{7}$$

The above equation can be written as:

$$\frac{d^2\psi}{d\varsigma^2} = k^2\psi, \tag{8}$$

where $k = \left(\frac{2n_0}{\varepsilon k_B T_{av}}\right)^{\frac{1}{2}} e z_v$.

The solution of equation (8) subjected to boundary conditions presented in Fig.1. is given as;

$$\psi = \zeta_1\left[\left(\frac{\frac{\zeta_2}{\zeta_1} - e^{-kd}}{2\sinh(kd)}\right)e^{ky} + \left(1 - \frac{\frac{\zeta_2}{\zeta_1} - e^{-kd}}{2\sinh(kd)}\right)e^{-ky}\right]. \tag{9}$$

Now using eq (4), (8) and (9), the mathematical expression for net charge density become [53]:

$$\rho_e = -\in k^2\xi_1 \times \left[\left(\frac{\frac{\xi_2}{\xi_1} - e^{-kl}}{2\sinh(kl)}\right)e^{k\zeta} + \left(1 + \frac{\frac{\xi_2}{\xi_1} - e^{-kl}}{2\sinh(kl)}\right)e^{-k\zeta}\right]. \tag{10}$$

For considered Casson fluid model, the constitutive equations are given as [54]:

$$\boldsymbol{\tau}_{ij} = \begin{bmatrix} \left(\mu_\in + \frac{p_\zeta}{\sqrt{2\boldsymbol{\pi}_a}}\right)2e_{ij},\ \boldsymbol{\pi}_a > \boldsymbol{\pi}_b \\ \left(\mu_\in + \frac{p_\zeta}{\sqrt{2\boldsymbol{\pi}_b}}\right)2e_{ij},\ \boldsymbol{\pi}_a < \boldsymbol{\pi}_b \end{bmatrix}, \tag{11}$$

Here

$\boldsymbol{\pi} = e_{ij}, e_{ij} : (i, j) -$ Deformation rate components,

$\boldsymbol{\pi}$: Product based on the non-Newtonian fluid,

$\boldsymbol{\pi}_b$: critical value for the product,

$\boldsymbol{\mu}_B$: Plastic dynamic viscosity,

p_ζ: Yield stress of the fluid.

Now the constitutive equations for thermal and concentration fields are:

$$\rho C_p \frac{\partial T}{\partial \tau} = -\nabla \cdot \overrightarrow{q}, \tag{12}$$

$$\overrightarrow{q} = -k\nabla T, \tag{13}$$

$$\frac{\partial C}{\partial \tau} = -\nabla \cdot \overrightarrow{\hbar}, \tag{14}$$

$$\overrightarrow{\hbar} = -D\nabla C, \tag{15}$$

In Eqs. (12)-(15), the terms ρ, T, C_p, K, q, C, $\hbar$, and D indicate fluid's density, fluid's temperature, specific heat capacitance, thermal conductivity, heat flux, concentration, diffusion flux, and mass diffusion coefficient respectively.

In view of Eq. (1) and incorporating Eq. (3), (10) and (11) in Eq. (2), we arrived at the mathematical governing form of momentum equation [54]:

$$\rho\frac{\partial u(\zeta,\tau)}{\partial t} = \mu\left(1 + \frac{1}{\chi}\right)\frac{\partial^2 u(\zeta,\tau)}{\partial\zeta^2} - \sigma B_0^2 u(\zeta,\tau) + \rho g\beta_T(T - T_s) + \rho g\beta_C(C - C_s) + E_x\rho_e, \tag{16}$$

and thermal and concentration field in compact form is given as under [10], [55]:

$$\rho C_p\frac{\partial T(\zeta,\tau)}{\partial\tau} = K\frac{\partial^2 T(\zeta,\tau)}{\partial\zeta^2}. \tag{17}$$

$$\frac{\partial C(\zeta,\tau)}{\partial\tau} = D\frac{\partial^2 C(\zeta,\tau)}{\partial\zeta^2}. \tag{18}$$

Subjected to the physical initial and boundary conditions:

$$\begin{aligned} u(\zeta,0) &= 0, \quad T(\zeta,0) = T_s, \\ u(0,\tau) &= 0, \quad T(0,\tau) = T_s, \\ u(l,\tau) &= U_0 H(\tau), \quad T(l,\tau) = T_s + (T_w - T_s)A\tau, \\ C(\zeta,0) &= C_s, \\ C(0,\tau) &= C_s, \\ C(l,\tau) &= C_s + (C_w - C_s)A\tau, \end{aligned} \tag{19}$$

In the governing equations the terms $\mu, B_0, \beta_T, \beta_C$ and χ indicates dynamic viscosity, the magnitude of the magnetic field, thermal expansion coefficient, concentration coefficient, and Casson fluid parameter respectively. In Eq.19

τ, ς, T_s, T_w, C_s, C_w and $H(\tau)$ shows time, y-axis, surrounding temperature, plate's temperature, constant concentration, concentration on the plate and Heaviside step function respectively.

III. NON-DIMENSIONALIZATION OF THE MATHEMATICAL MODEL

This section of the article shows how to convert a dimensional model into a non-dimensional model. Primarily, the dimensional governing equations have been non-dimensionalized by removing units and reducing variables using relative non-similarity variables. For this purpose, the following similarity variables have been introduced.

$$u^{\cdot} = \frac{u}{u_s}, \quad \tau^{\cdot} = \frac{\upsilon}{l^2}\tau, \quad \zeta^{\cdot} = \frac{\zeta}{l}, \quad \Theta = \frac{T - T_s}{T_w - T_s},$$
$$\Phi = \frac{C - C_s}{C_w - C_s}, \quad k^{\cdot} = kl, \quad \Re_{\xi} = \frac{\xi_2}{\xi_1},$$
$$\lambda = \frac{ql}{k\,(T_w - T_s)}, \quad \eta = \frac{jl}{D\,(C_w - C_s)}, \quad A = \frac{v}{l^2}. \tag{20}$$

Incorporating these similarity variables into the Eqs. (16)-(18), and ignoring the notion $(\cdot)$ the governing equations will take the form:

$$\frac{\partial u(\zeta,\tau)}{\partial \tau} = \left(1 + \frac{1}{\chi}\right)\frac{\partial^2 u(\zeta,\tau)}{\partial \zeta^2} - Mu(\zeta,\tau) + Gr\Theta(\zeta,\tau) + Gm\Phi(\zeta,\tau) + k^2\left(A_1 e^{k\zeta} + A_2 e^{-k\zeta}\right), \tag{21}$$

$$\frac{\partial \Theta(\zeta,\tau)}{\partial \tau} = \frac{1}{\Pr}\frac{\partial^2 \Theta(\zeta,\tau)}{\partial \zeta^2}, \tag{22}$$

$$\frac{\partial \Phi(\zeta,\tau)}{\partial \tau} = \frac{1}{Sc}\frac{\partial^2 \Phi(\zeta,\tau)}{\partial \zeta^2}, \tag{23}$$

And the associated dimensionless conditions are:

$$\left.\begin{array}{lll} u(\zeta,0) = 0, & T(\zeta,0) = 0, & C(\zeta,0) = 0, \\ u(0,\tau) = 0, & T(0,\tau) = 0, & C(0,\tau) = 0, \\ u(1,\tau) = H(\tau), & T(l,\tau) = \tau, & C(l,\tau) = \tau, \end{array}\right\}. \tag{24}$$

In the dimensionless variables $u_s = \frac{\epsilon\xi_1 E_x}{\mu}$, k, $k^{\cdot}$ and $\Re_{\xi}$ represent Helmholtz-Smoluchowski velocity, Debye-Huckel parameter, relative micro-channel ratio and the ratio of the zeta potential of the walls while in the governing equations, the term $M = \frac{\sigma B_0^2 l^2}{\mu}$, $Gr = \frac{gl\beta_T(T_w - T_s)}{\upsilon u_s}$, $Gm = \frac{gl\beta_C(C_w - C_s)}{\upsilon u_s}$, $Sc = \frac{\upsilon}{D}$ and $\Pr = \frac{\mu C_p}{K}$ shows the magnetic number, thermal Grashof number, mass Grashof number, Schmidt number, and Prandtl number respectively. $A_1 = \frac{R_{\xi} - e^{-k}}{2\sinh(k)}$ and $A_2 = 1 - A_1$ are constant.

IV. DISCRETIZATION OF THE MATHEMATICAL MODEL

This section of the manuscript is focused on the discretization of the proposed mathematical model. Before going to discretize the model, first, we will transform the local model to a fractal-fractional model with an exponential kernel. Employing the fractal-fractional operator of Caputo-Fabrizio, Eqs. (21)-(23) will take the shape:

$${}^{FF}_{0}\wp^{\alpha}_{\tau} u(\zeta,\tau) = \beta\tau^{\beta-1}\left\{\begin{array}{l}\left(1 + \frac{1}{\chi}\right)\frac{\partial^2 u(\zeta,\tau)}{\partial \zeta^2} \\ - Mu(\zeta,\tau) + Gr\Theta(\zeta,\tau) \\ + Gm\Phi(\zeta,\tau) \\ + k^2\left(A_1 e^{k\zeta} + A_2 e^{-k\zeta}\right)\end{array}\right\}$$

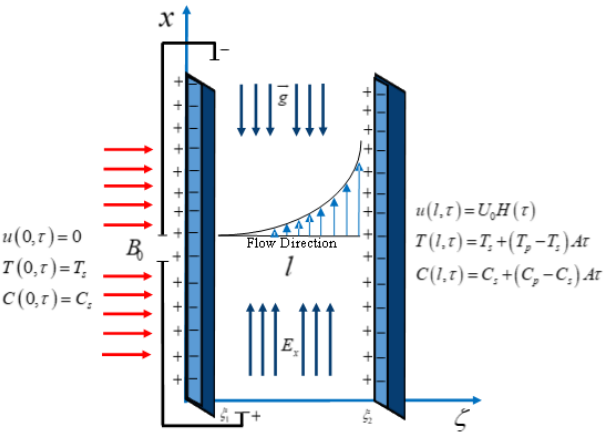

FIGURE 1. Physical view of casson fluid flow with electro-osmotic phenomena.

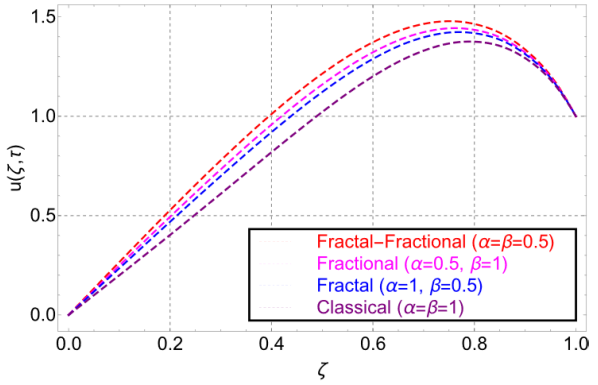

FIGURE 2. Velocity comparison of fractal-fractional, fractional, fractal and classical order.

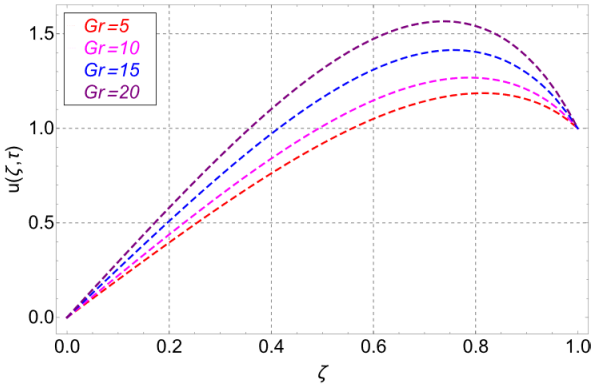

FIGURE 3. Influence of Gr on velocity profile while other parameters are $Gm = 15$, $\chi = 2$, $\Pr = 15$, $k = 1.5$, $Sc = 15$, $R_{\xi} = 1.5$ and $t = \alpha = \beta = 0.5$.

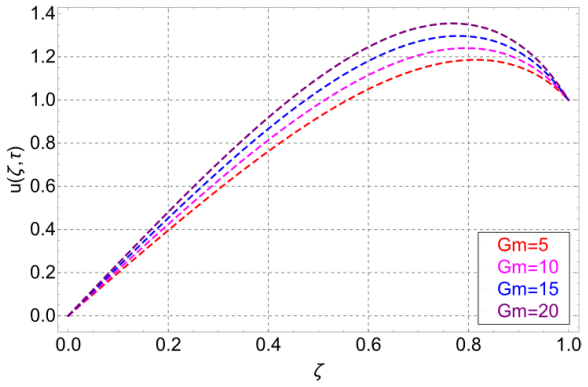

FIGURE 4. Influence of Gm on velocity profile while other parameters are $Gr = 15$, $\chi = 2$, $\mathrm{Pr} = 15$, $k = 1.5$, $Sc = 15$, $R_\xi = 1.5$ and $t = \alpha = \beta = 0.5$.

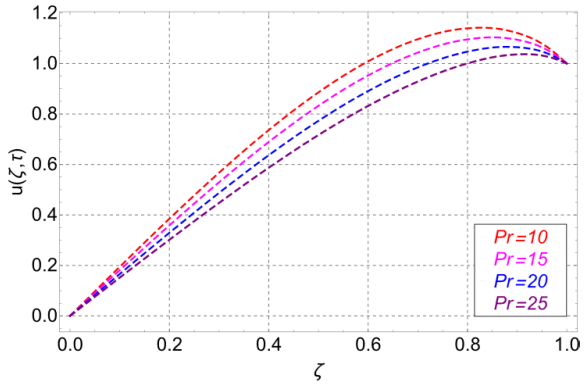

FIGURE 5. Influence of Pr on velocity profile while other parameters are $Gr = 15$, $Gr = 15$, $\chi = 2$, $k = 1.5$, $Sc = 15$, $R_\xi = 1.5$ and $t = \alpha = \beta = 0.5$.

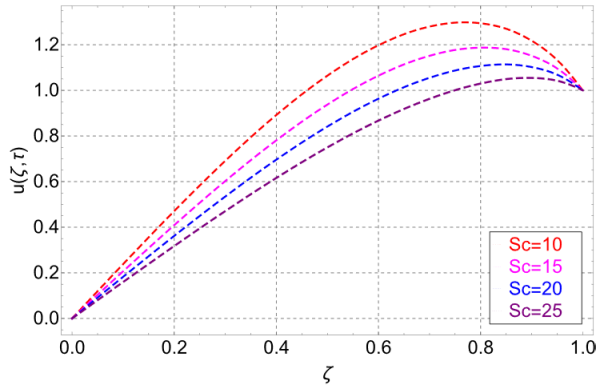

FIGURE 6. Influence of Sc on velocity profile while other parameters are $Gr = 15$, $Gm = 15$, $\chi = 2$, $k = 1.5$, $\mathrm{Pr} = 15$, , $R_\xi = 1.5$ and $t = \alpha = \beta = 0.5$.

$$- \frac{u(\zeta, 0)}{\Gamma(1-\alpha)} \tau^{-\alpha}, \tag{25}$$

$${}^{FF}_{0}\wp^{\alpha}_{\tau}\Theta(\zeta,\tau) = \beta\tau^{\beta-1}\left\{\frac{1}{\mathrm{Pr}}\frac{\partial^2\Theta(\zeta,\tau)}{\partial\zeta^2}\right\} - \frac{\Theta(\zeta,0)}{\Gamma(1-\alpha)}\tau^{-\alpha}, \tag{26}$$

$${}^{FF}_{0}\wp^{\alpha}_{\tau}\Phi(\zeta,\tau) = \beta\tau^{\beta-1}\left\{\frac{1}{Sc}\frac{\partial^2\Phi(\zeta,\tau)}{\partial\zeta^2}\right\}$$

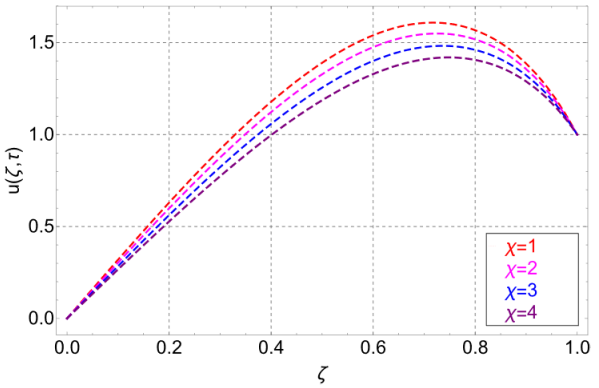

FIGURE 7. Influence of χ on velocity profile while other parameters are $Gr = 15$, $Gm = 15$, $\mathrm{Pr} = 15$, $k = 1.5$, $Sc = 15$, $R_\xi = 1.5$ and $t = \alpha = \beta = 0.5$.

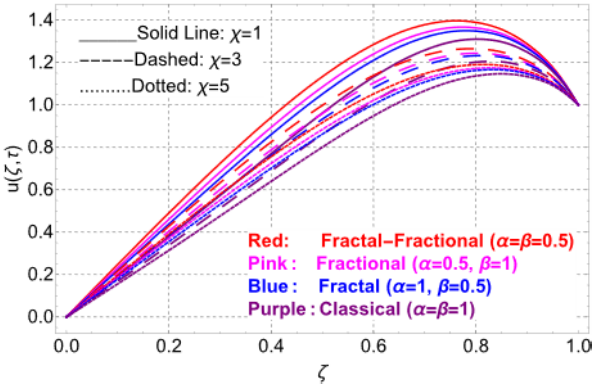

FIGURE 8. Influence of χ on fractal-fractional, fractional, fractal and classical order velocity when $Gr = 15$, $Gm = 15$, $\mathrm{Pr} = 15$, $k = 1.5$, $Sc = 15$, $R_\xi = 1.5$ and $t = 1$.

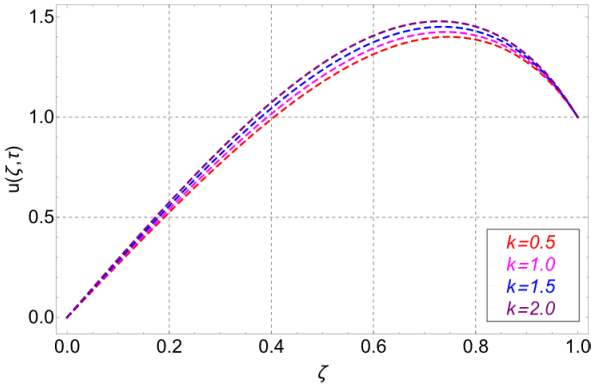

FIGURE 9. Influence of k on velocity profile while other parameters are $Gr = 15$, $Gm = 15$, $\chi = 2$, $\mathrm{Pr} = 15$, $Sc = 15$, $R_\xi = 1.5$ and $t = \alpha = \beta = 0.5$.

$$- \frac{\Phi(\zeta, 0)}{\Gamma(1-\alpha)} \tau^{-\alpha}, \tag{27}$$

In the light of the aforementioned initial conditions, Eqs. (25)-(27) will take the form;

$${}^{FF}_{0}\wp^{\alpha}_{\tau}u(\zeta,\tau) = \beta\tau^{\beta-1}\left\{\begin{array}{l}\left(1+\frac{1}{\chi}\right)\frac{\partial^2 u(\zeta,\tau)}{\partial\zeta^2} \\ -Mu(\zeta,\tau) \\ +Gr\Theta(\zeta,\tau)+Gm\Phi(\zeta,\tau) \\ +k^2\left(A_1e^{k\zeta}+A_2e^{-k\zeta}\right)\end{array}\right\}, \tag{28}$$

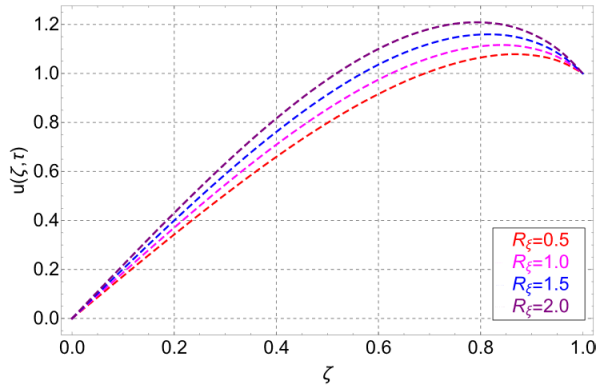

FIGURE 10. Influence of R_ξ on velocity profile while other parameters are $Gr = 15$, $Gm = 15$, $\chi = 2$, $k = 1.5$, $\mathrm{Pr} = 15$, , $Sc = 15$ and $t = \alpha = \beta = 0.5$.

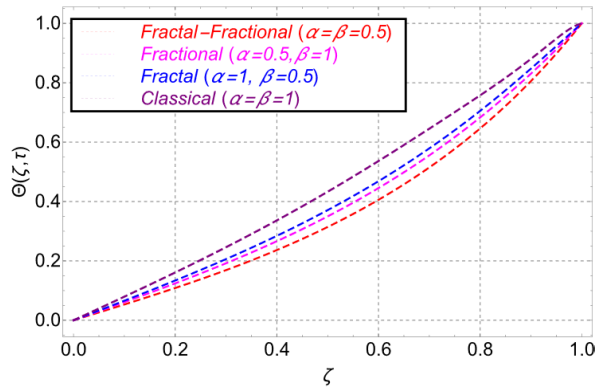

FIGURE 11. Temperature comparison of fractal-fractional, fractional, fractal and classical order.

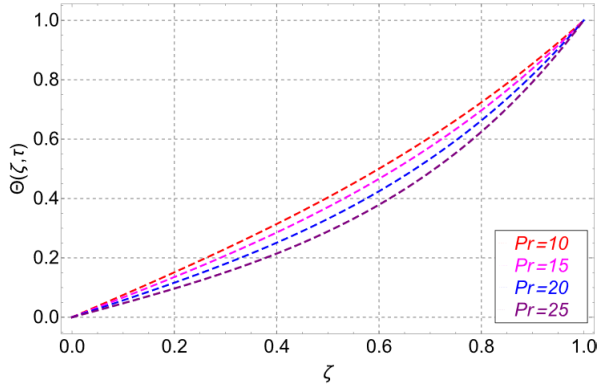

FIGURE 12. Influence of Pr on temperature profile while other parameters are $\alpha = \beta = 0.5$ and $\tau = 1$.

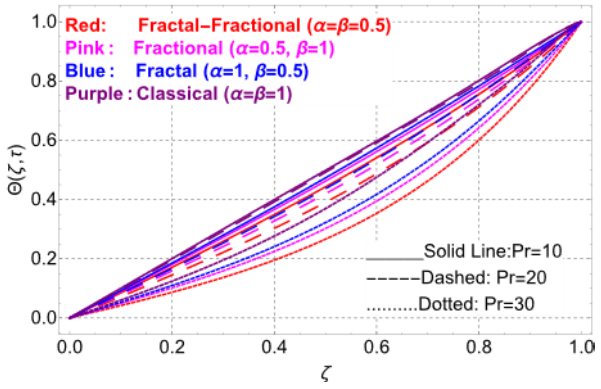

FIGURE 13. Influence of Pr on fractal-fractional, fractional, fractal and classical order temperature distribution.

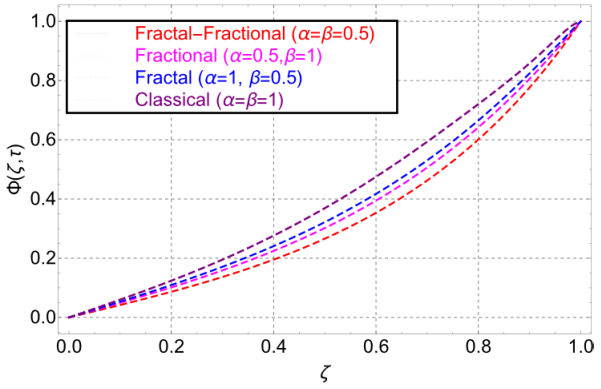

FIGURE 14. Concentration comparison of fractal-fractional, fractional, fractal and classical order.

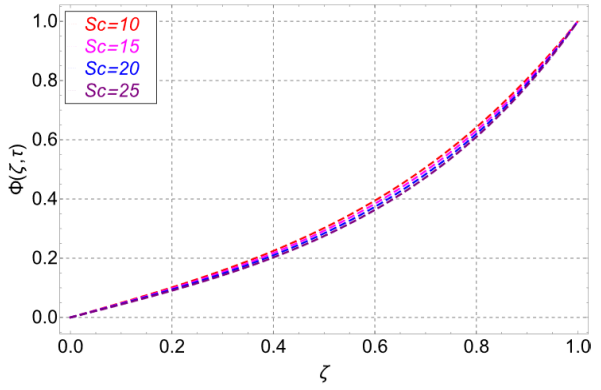

FIGURE 15. Influence of Sc on concentration profile while other parameters and $\alpha = \beta = 0.5$ and $\tau = 1$.

$$ {}^{FF}_{0}\wp^{\alpha}_{\tau}\Theta(\zeta,\tau) = \beta\tau^{\beta-1}\left\{\frac{1}{\mathrm{Pr}}\frac{\partial^2\Theta(\zeta,\tau)}{\partial\zeta^2}\right\}, \tag{29} $$

$$ {}^{FF}_{0}\wp^{\alpha}_{\tau}\Phi(\zeta,\tau) = \beta\tau^{\beta-1}\left\{\frac{1}{Sc}\frac{\partial^2\Phi(\zeta,\tau)}{\partial\zeta^2}\right\}. \tag{30} $$

Here ${}^{FF}_{a}\wp^{\alpha,\beta}_{\tau}$ is the fractal-fractional operator of the exponential kernel [21], [24] is given as;

$$ {}^{FF}_{a}\wp^{\alpha,\beta}_{\tau}\varpi(\tau) = \frac{N(\alpha)}{\Gamma(1-\alpha)}\frac{d}{d\tau^{\beta}}\int_{a}^{\tau}\varpi(\zeta) \times \exp\left\{-\frac{\alpha}{1-\alpha}(\tau-\zeta)\right\}d\zeta, \tag{31} $$

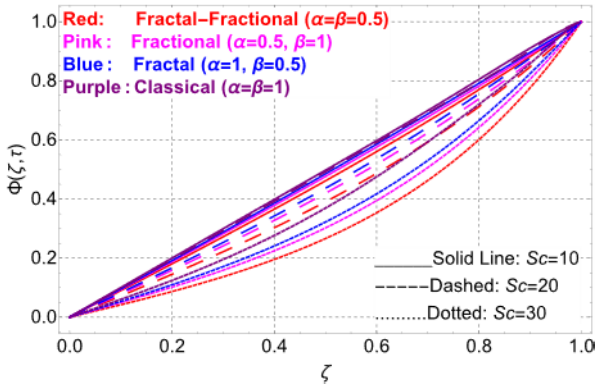

FIGURE 16. Influence of Sc on fractal-fractional, fractional, fractal and classical order concentration distribution.

Eq. (31) follows the following property;

$$N(0) = N(1) = 1.$$

where $\varpi(\tau)$ be differentiable in the open interval (a, b), ϖ is fractally differentiable on (a, b) with the order β.

Determine the exact solution to the fractal-fractional model is extremely difficult for researchers. As a result, the solution of the fractal-fractional model will be handled using the finite difference (Crank-Nicolson) scheme in the current work. The Crank-Nicolson scheme is used to discretize the fractal-fractional order model.

The first order fractal-fractional order derivative can be discretized using the Crank-Nicolson approach as;

$$\begin{aligned} &{}^{FF}_{0}\wp^{\alpha}_{\tau}\varpi(\zeta,\tau) \\ &= \beta\tau^{\beta-1}\frac{N(\alpha)}{2\alpha}\left\{\frac{\varpi_i^{j+1}-\varpi_i^{j}}{\lambda} + \sum_{j=1}^{m}\left(\frac{\varpi_i^{j+1-m}-\varpi_i^{j-m}}{\lambda} + O(\tau)\right)\right\} \\ &\quad \times \delta_{j,m}, \end{aligned} \tag{32}$$

where $\delta_{j,m} = erf\left\{\frac{\alpha j}{1-\alpha}(m-j)\right\} - erf\left\{\frac{\alpha j}{1-\alpha}(m-j+1)\right\}$

The function's second-order derivative can be discretized using the Crank-Nicolson approach, as shown below;

$$\begin{aligned} &\frac{\partial^2\varpi(\zeta,\tau)}{\partial\zeta^2} \\ &= \left\{\frac{\left(\varpi_{i+1}^{j+1} - 2\varpi_i^{j+1} + \varpi_{i-1}^{j+1}\right) + \left(\varpi_{i+1}^{j} - 2\varpi_i^{j} + \varpi_{i-1}^{j}\right)}{2h^2}\right\} \\ &\quad + O(\tau), \end{aligned} \tag{33}$$

Keeping in view the above discretization defined in Eq. (32)-(33), the fractal-fractional Caputo-Fabrizio governing equations will take the form:

$$\begin{aligned} &\frac{N(\alpha)}{2\alpha}\left\{\frac{\varpi_i^{j+1}-\varpi_i^{j}}{\lambda} + \sum_{j=1}^{m}\left(\frac{\varpi_i^{j+1-m}-\varpi_i^{j-m}}{\lambda}\right)\right\}\delta_{j,m} \\ &= \beta t^{\beta-1}\left\{\begin{array}{l}\left(1+\frac{1}{\chi}\right)\left(\frac{\left(u_{i+1}^{j+1} - 2u_i^{j+1} + u_{i-1}^{j+1}\right)}{2h^2} + \frac{\left(u_{i+1}^{j} - 2u_i^{j} + u_{i-1}^{j}\right)}{2h^2}\right) \\ -\frac{1}{2}\left(\begin{array}{l}M\left(u_i^{j+1}+u_i^{j}\right) \\ +Gr\left(\Theta_i^{j+1}+\Theta_i^{j}\right) \\ +Gm\left(\Phi_i^{j}++\Phi_i^{j}\right)\end{array}\right) \\ +k^2\left((A_1+A_2)\left(e^{-kj}\left(1-e^{-k}\right)\right)\right)\end{array}\right\}, \end{aligned} \tag{34}$$

$$\begin{aligned} &\frac{N(\alpha)}{2\alpha}\left\{\frac{\Theta_i^{j+1}-\Theta_i^{j}}{\lambda} + \sum_{j=1}^{m}\left(\frac{\Theta_i^{j+1-m}-\Theta_i^{j-m}}{\lambda}\right)\right\}\delta_{j,m} \\ &= \beta\tau^{\beta-1}\left\{\frac{1}{2h^2}\left(\frac{1}{\mathrm{Pr}}\right)\left(\begin{array}{l}\left(\Theta_{i+1}^{j+1} - 2\Theta_i^{j+1} + \Theta_{i-1}^{j+1}\right) \\ +\left(\Theta_{i+1}^{j} - 2\Theta_i^{j} + \Theta_{i-1}^{j}\right)\end{array}\right)\right\}, \end{aligned} \tag{35}$$

$$\begin{aligned} &\frac{N(\alpha)}{2\alpha}\left\{\frac{\Phi_i^{j+1}-\Phi_i^{j}}{\lambda} + \sum_{j=1}^{m}\left(\frac{\Phi_i^{j+1-m}-\Phi_i^{j-m}}{\lambda}\right)\right\}\delta_{j,m} \\ &= \beta\tau^{\beta-1}\left\{\frac{1}{2h^2}\left(\frac{1}{Sc}\right)\left(\begin{array}{l}\left(\Phi_{i+1}^{j+1} - 2\Phi_i^{j+1} + \Phi_{i-1}^{j+1}\right) \\ +\left(\Phi_{i+1}^{j} - 2\Phi_i^{j} + \Phi_{i-1}^{j}\right)\end{array}\right)\right\}. \end{aligned} \tag{36}$$

along with the boundary conditions given in Eq. (13). Assume that $y_i = ih$, $0 \le i \le M$ with $Mh = 1$ and $t_j = j\lambda$, $0 \le j \le Q$. here h and λ indicates the space and time step length while M and Q represents the number of grids points.

A. SKIN FRICTION

In dimensionless form the skin friction is given as:

$$S_f = \left(1+\frac{1}{\chi}\right)\left.\frac{\partial u}{\partial\varsigma}\right|_{\varsigma=0} \tag{37}$$

B. NUSSELT NUMBER

In dimensionless form the Nusselt Number is given as:

$$Nu = -k\left.\frac{\partial\Theta}{\partial\varsigma}\right|_{\varsigma=0}. \tag{38}$$

C. SHERWOOD NUMBER

In dimensionless form the Sherwood Number is given as:

$$S_h = -D\left(\frac{\partial\Phi}{\partial\varsigma}\right)_{\varsigma=0}. \tag{39}$$

V. GRAPHICAL ANALYSIS

This section of the article focused on the physical aspect of the proposed fractal-fractional Caputo-Fabrizio model. Fractal-fractional Casson fluid flow has been examined in

TABLE 1. Variation in skin friction against different embedded parameters.

Gr	Gm	Pr	Sc	χ	k	M	α	β	S_f
5	5	10	10	2	2	0.5	0.5	0.5	**2.638**
10	5	10	10	2	2	0.5	0.5	0.5	**2.562**
5	**10**	10	10	2	2	0.5	0.5	0.5	**2.598**
5	5	**12**	10	2	2	0.5	0.5	0.5	**2.641**
5	5	10	**12**	2	2	0.5	0.5	0.5	**2.646**
5	5	10	10	**3**	2	0.5	0.5	0.5	**2.642**
5	5	10	10	2	**3**	0.5	0.5	0.5	**2.637**
5	5	10	10	2	2	**0.8**	0.5	0.5	**2.681**
5	5	10	10	2	2	0.5	**0.8**	0.5	**2.673**
5	5	10	10	2	2	0.5	0.5	**0.8**	**2.679**

TABLE 2. Variation in Nusselt number against different embedded parameters.

Pr	τ	α	β	Nu
10	1	0.5	0.5	**1.537**
12	1	0.5	0.5	**1.533**
10	**2**	0.5	0.5	**1.599**
10	1	**0.8**	0.5	**1.532**
10	1	0.5	**0.8**	**1.535**

TABLE 3. Variation in Sherwood number against different embedded parameters.

Sc	τ	α	β	S_h
10	1	0.5	0.5	**3.293**
12	1	0.5	0.5	**3.291**
10	**2**	0.5	0.5	**3.312**
10	1	**0.8**	0.5	**3.282**
10	1	0.5	**0.8**	**2.289**

the vertical microchannel of the length l. The phenomenon of electro-osmotic and the effect of the magnetic field also has been taken into the account. A numerical solution has been obtained for the fractal-fractional governing equations via discretization of the Crank-Nicolson scheme. For the insight view of the phenomenon, graphs for the rooted parameters have been drawn.

The comparison of the fractal-fractional, fractional, and classical order models for velocity distribution is shown in Fig.2. The graphic clearly shows that the fractal-fractional model has a greater memory impact than the fractional-order and classical models. This property of the fractal-fractional model is due to the fractal parameter, which is not present in the fractional and classical models. The fractal-fractional model is more convenient and realistic to real-world phenomena because of the larger memory effect. It also gives more than one fluid layer allowing experimentalists to compare their work in one of the layers that are best adapted to their work by modifying the fractal-fractional parameter. Figure 3 depicts the flow behavior against the thermal Grashof number Gr. The velocity profile demonstrates an increase in response to increasing Gr values. The fluid near the plate warms up as the magnitude of Gr increases, causing bouncy forces to arise in the fluid, making the fluid less dense and decreasing the viscous forces, resulting in an accelerated fluid motion. Figure 4 depicts the effects of mass Grashof number Gm on fluid motion. The graphic clearly shows that raising the magnitude of Gm causes the velocity field to increase. The reasoning behind this increase is that when the value of Gm rises, the concentration of particles in the fluid increases, allowing the fluid motion to accelerate. Figure 5 depicts the effect of the Prandtl. number Pr. It can be shown that when the Prandtl number increases, fluid velocity falls. Because it is a ratio of viscous forces to thermal forces. While raising the Pr value, the viscous forces appear to be dominant over the thermal forces, resulting in a drop in fluid velocity. While Fig.6 shows variation in velocity field in response to Schmidt number Sc. the Velocity profile shows retardation in its behavior as the value of Sc increase. This is due to the diffusion rate which decreases by increasing the value of Sc and as a result fluid motion slows down. Figure 7 depicts the behavior of the velocity field in the reaction of the material parameter χ. Figure 7 depicts a fall in fluid velocity as the value χ increases. This fluid behavior is physically correct since increasing the magnitude of the material parameter increases the viscous forces in the fluid, causing the fluid to slow down. The same behavior of χ can be seen for fractional-fractal, fractional, fractal and classical order velocity distribution in figure 8. The upshots of the electro-kinetic parameter k on velocity variation are drawn in Fig.9. Fig. 9 shows an increase in the velocity field of the fluid in response to greater values k. the logic behind this variation is quite clear because the greater magnitude of k makes thinner the electric double layer (EDL) and as a result, electro osmotic flow of the fluid accelerates. Fig.10 has been drawn to check variation in the velocity field of electro-osmotic flow against asymmetric zeta potential R_ξ. Zeta potential R_ξ is also related to the EDL of the electro-osmotic flow of the Casson fluid. as the magnitude of R_ξ increases, the EDL becomes thinner as a result the drag forces in the fluid decrease which accelerates the fluid motion.

Fig.11. reveals a comparative analysis of fractal, fractal-fractional, fractional and classical order on the variation of the thermal field. It is quite clear from the figure that fractal-fractal has a greater memory effect as compared to the fractal, fractional, and classical order. This greater memory effect is due to the extra fractal dimension included in the

TABLE 4. Variation in velocity profile against ζ for different values of Casson parameter χ when $Gr = Gm = k = 0$.

	Results of Sheikh et al. [54]				Present Results			
ζ	$u(\zeta,\tau)$ at $\chi = 0.1$	$u(\zeta,\tau)$ at $\chi = 0.9$	$u(\zeta,\tau)$ at $\chi = 3$	$u(\zeta,\tau)$ at $\chi = 9$	$u(\zeta,\tau)$ at $\chi = 0.1$	$u(\zeta,\tau)$ at $\chi = 0.9$	$u(\zeta,\tau)$ at $\chi = 3$	$u(\zeta,\tau)$ at $\chi = 9$
0	0	0	0	0	0	0	0	0
0.04	0.04	0.042	0.045	0.048	0.04	0.042	0.044	0.046
0.08	0.08	0.084	0.09	0.095	0.08	0.083	0.089	0.092
0.12	0.12	0.126	0.135	0.142	0.12	0.125	0.133	0.140
0.16	0.16	0.168	0.18	0.19	0.16	0.166	0.179	0.188
0.2	0.2	0.21	0.225	0.236	0.2	0.209	0.223	0.235
0.24	0.24	0.251	0.269	0.283	0.24	0.249	0.265	0.280
0.28	0.28	0.293	0.313	0.329	0.28	0.90	0.31	0.325
0.32	0.321	0.334	0.357	0.374	0.32	0.331	0.354	0.371
0.36	0.361	0.376	0.4	0.419	0.36	0.372	0.397	0.414
0.4	0.401	0.417	0.443	0.463	0.40	0.414	0.441	0.46
0.44	0.441	0.458	0.486	0.507	0.44	0.454	0.484	0.503
0.48	0.481	0.498	0.528	0.55	0.481	0.494	0.525	0.547
0.52	0.521	0.539	0.569	0.591	0.521	0.534	0.565	0.588
0.56	0.561	0.579	0.609	0.632	0.561	0.575	0.604	0.629
0.6	0.601	0.619	0.649	0.672	0.60	0.613	0.645	0.667
0.64	0.641	0.659	0.688	0.711	0.64	0.656	0.684	0.708
0.68	0.681	0.698	0.727	0.748	0.68	0.696	0.724	0.744
0.72	0.721	0.737	0.764	0.785	0.72	0.734	0.762	0.782
0.76	0.761	0.776	0.801	0.82	0.76	0.773	0.799	0.817
0.8	0.801	0.814	0.837	0.854	0.80	0.812	0.834	0.851
0.84	0.84	0.852	0.872	0.886	0.84	0.85	0.869	0.882
0.88	0.88	0.89	0.905	0.917	0.88	0.888	0.903	0.912
0.92	0.92	0.927	0.938	0.946	0.92	0.924	0.935	0.943
0.96	0.96	0.964	0.97	0.974	0.96	0.963	0.968	0.972
1	1	1	1	1	1	1	1	1

fractional derivative definition. The behavior is the same as observed in Fig.2. The behavior of the thermal field in response to the Prandtl number Pr is plotted in Fig.12. Decay in the thermal field can be noticed from the figure for the greater value of Pr. Prandtl number is inversely related to the thermal forces of the fluid so as the Pr increase the thermal forces decrease and consequently thermal field declines. In addition to that, the influence of Pr for the fractional-fractal, fractal, fractional and classical order temperature field is also displayed in Fig.13. The same behavior as Fig.12 can be seen in Fig.13 for different fractal and fractional orders.

Fig.14. displays a comparison of fractal, fractal-fractional, fractional, and classical order on the variations of the concentration field. The same behavior for the memory effect is observed as noticed in Fig.2 and Fig.11. Fig.15. illustrates the impact of Schmidt number *Sc* on the concentration field. From the graph, a decline in the concentration field can be seen for larger values of *Sc*. It is quite obvious because the *Sc* has inversely related to the mass diffusion rate. As the magnitude of *Sc* increases, the concentration field shows the decay in its behavior. Additionally, the behavior of concentration profile for different values of *Sc* indifferent cases i.e., fractal-fractional, fractional, fractal and classical order can be seen in Fig. 16 which shows the identical behavior as Fig.15 for different fractional and fractal orders.

In order to validate the present study, the present analysis is compared with the exact solutions of Casson fluid model published by Sheikh *et al.* [54] which can be seen in Fig.17. Our model is the general case of the published work of Sheikh *et al.* [54] and the model presented by Sheikh *et al.* [54]. can be recovered from the present problem by considering $Gr \rightarrow 0$, $Gm \rightarrow 0$ and $k \rightarrow 0$. It can be seen from the comparative figure that our results are in excellent agreement with the exact solutions of Sheikh *et al.* [54] which validates our results achieved via numerical method. The comparison of present results and results of Sheikh *et al.* [54] is also given in tabular form in table 4. From the table values, it can be observed that the present analysis is in good agreement with the published work and the numerical results of the current study matches with the published results which validates the correctness of the present work.

In order to validate the present results and the implemented numerical technique, the grid sensitivity analysis is also performed which can be seen in Figs. 18-20. From these figures, it can be noticed that the present numerical algorithm gives us the correct results for any step-size *h*. As, the used numerical

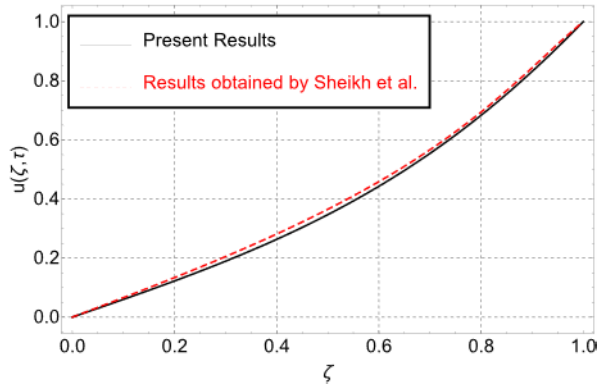

FIGURE 17. Comparison of the present results with the published results of Sheikh *et al.* [54] when Pr = 15, $Sc = 15$, $R_\xi = 1.5$, $t = \alpha = \beta = 0.5$ and $Gr = Gm = k = 0$.

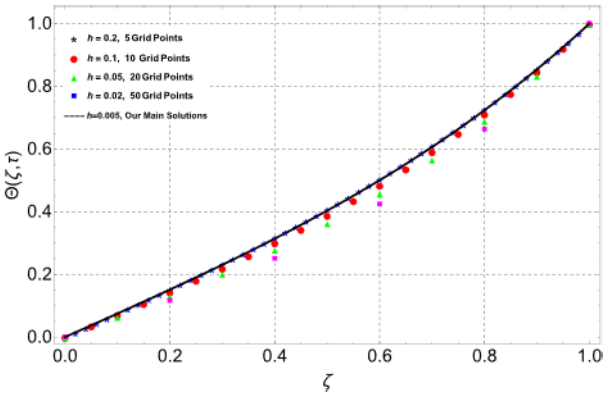

FIGURE 19. Grid sensitivity analysis of temperature profile for different values of step-size h.

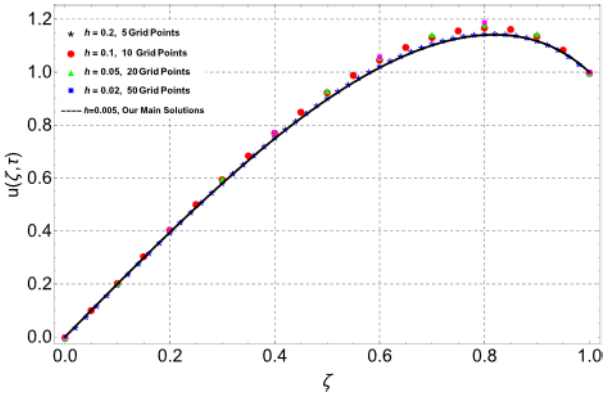

FIGURE 18. Grid sensitivity analysis of velocity profile for different values of step-size h.

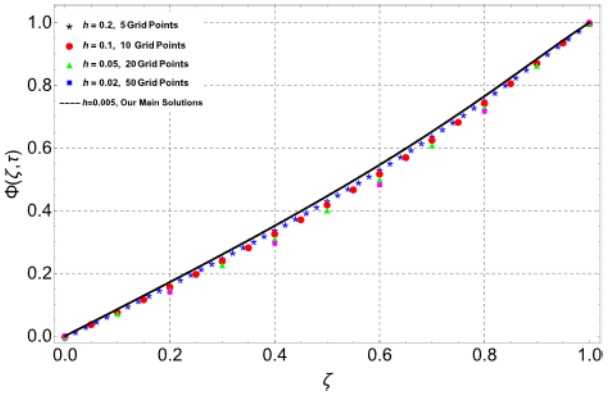

FIGURE 20. Grid sensitivity analysis of concentration profile for different values of step-size h.

algorithm i.e., Crank-Nicolson finite difference scheme is unconditionally stable and it gives correct and true results for any value of h which means that if we increase or decrease the grid points, it doesn't affect the results which can also be seen from the figures. By varying the value of step-size h, it doesn't affect the behavior of the flow or thermal boundary layer which validates the correctness of the present numerical method which is sufficient for the authentication of the present numerical algorithm.

In the present analysis, the variation in Skin friction, Nusselt number and Sherwood number is also calculated from the solutions by using the expressions given in Eq. (31)-(33). The variation in Skin friction in response to different embedded parameters is given in numerical form in Table 1 while the variation in Nusselt and Sherwood numbers are tabulated in Tables 2 and 3 respectively.

VI. CONCLUDING REMARKS

Fractal-Fractional model of Casson fluid with the impact of electro-osmotic phenomena has been analyzed numerically with the approach of Crank-Nicolson scheme. The analysis of the flow has been done in the microchannel of length l. Primally, the local mathematical model has been non-dimensional with the help of non-dimensional quantities and then transformed into a fractal-fractional model via the operator of Caputo-Fabrizio derivative. The numerical solution of the proposed fractal-fractional model has been obtained via the finite difference approach (Crank-Nicolson). Graphs have been plotted via computational software and illustrated physically. The key observations from the analysis are listed below:

- When compared to the fractional-order and the classical model, the fractal-fractional order model has a significant memory effect. This feature in the fractal-fractional derivative is because of the fractal dimension which is not held by any fractional and classical model. The fractal-fractional model is handier and more realistic to the real-world phenomena due to the higher memory effect.
- It has been reported that velocity field increase with the larger values of Gr, Gm, k and $\Re_\xi$ while decreasing with greater values of the parameters Pr, Sc, M and χ.
- The temperature field shows a decline in response to Pr.
- Concentration field enhances with the increasing magnitude of Sc.

REFERENCES

[1] A. Atangana and I. Koca, "Chaos in a simple nonlinear system with Atangana–Baleanu derivatives with fractional order," *Chaos, Solitons Fractals*, vol. 89, pp. 447–454, Aug. 2016, doi: 10.1016/J.CHAOS.2016.02.012.

[2] R. Metzler, W. Schick, H. G. Kilian, and T. F. Nonnenmacher, "Relaxation in filled polymers: A fractional calculus approach," *J. Chem. Phys.*, vol. 103, no. 16, p. 7180, Jun. 1998, doi: 10.1063/1.470346.

[3] Q. Al-Mdallal, K. A. Abro, and I. Khan, "Analytical solutions of fractional Walter's b fluid with applications," *Complexity*, vol. 2018, pp. 1–10, 2018, doi: 10.1155/2018/8131329.

[4] N. Sebaa, Z. E. A. Fellah, W. Lauriks, and C. Depollier, "Application of fractional calculus to ultrasonic wave propagation in human cancellous bone," *Signal Process.*, vol. 86, no. 10, pp. 2668–2677, Oct. 2006, doi: 10.1016/J.SIGPRO.2006.02.015.

[5] P. Ostalczyk, *Discrete Fractional Calculus*, vol. 4. Singapore: World Scientific, Jan. 2016, doi: 10.1142/9833.

[6] R. L. Magin and M. Ovadia, "Modeling the cardiac tissue electrode interface using fractional calculus," *J. Vibrat. Control*, vol. 14, nos. 9–10, pp. 1431–1442, Sep. 2008, doi: 10.1177/1077546307087439.

[7] Z. Ahmad, M. Arif, F. Ali, I. Khan, and K. S. Nisar, "A report on COVID-19 epidemic in Pakistan using SEIR fractional model," *Sci. Rep.*, vol. 10, no. 1, pp. 1–14, Dec. 2020, doi: 10.1038/s41598-020-79405-9.

[8] Z. Ahmad, M. Arif, and I. Khan, "Dynamics of fractional order SIR model with a case study of COVID-19 in Turkey," *CITY Univ. Int. J. Comput. Anal.*, vol. 4, no. 1, pp. 19–37, 2020, doi: 10.33959/CUIJCA.V4I01.43.

[9] M. Sinan, K. Shah, P. Kumam, I. Mahariq, K. J. Ansari, Z. Ahmad, and Z. Shah, "Fractional order mathematical modeling of typhoid fever disease," *Results Phys.*, vol. 32, Jan. 2022, Art. no. 105044, doi: 10.1016/j.rinp.2021.105044.

[10] S. Murtaza, F. Ali, N. A. Sheikh, I. Khan, and K. S. Nisar, "Analysis of silver nanoparticles in engine oil: Atangana–Baleanu fractional model," *Comput., Mater. Continua*, vol. 67, no. 3, pp. 2915–2932, 2021, doi: 10.32604/CMC.2021.013757.

[11] F. Ali, S. Murtaza, I. Khan, N. A. Sheikh, and K. S. Nisar, "Atangana–Baleanu fractional model for the flow of Jeffrey nanofluid with diffusion-thermo effects: Applications in engine oil," *Adv. Differ. Equ.*, vol. 2019, no. 1, pp. 1–21, Dec. 2019, doi: 10.1186/s13662-019-2222-1.

[12] F. Ali, Z. Ahmad, M. Arif, I. Khan, and K. S. Nisar, "A time fractional model of generalized Couette flow of couple stress nanofluid with heat and mass transfer: Applications in engine oil," *IEEE Access*, vol. 8, pp. 146944–146966, 2020, doi: 10.1109/ACCESS.2020.3013701.

[13] Z. Ahmad, F. Ali, A. M. Alqahtani, N. Khan, and I. Khan, "Dynamics of cooperative reactions based on chemical kinetics with reaction speed: A comparative analysis with singular and nonsingular kernels," *Fractals*, vol. 2021, Dec. 2021, Art. no. 2240048, doi: 10.1142/S0218348X22400485.

[14] K. A. Abro, A. A. Memon, and M. A. Uqaili, "A comparative mathematical analysis of RL and RC electrical circuits via Atangana–Baleanu and Caputo-Fabrizio fractional derivatives," *Eur. Phys. J. Plus*, vol. 133, no. 3, pp. 1–9, Mar. 2018, doi: 10.1140/EPJP/I2018-11953-8.

[15] T. F. Nonnenmacher and R. Metzler, "On the Riemann-Liouville fractional calculus and some recent applications," *Fractals*, vol. 3, no. 3, pp. 557–566, Nov. 2011, doi: 10.1142/S0218348X95000497.

[16] M. Caputo, "Linear models of dissipation whose Q is almost frequency independent-II," *Geophys. J. Int.*, vol. 13, no. 5, pp. 529–539, Nov. 1967, doi: 10.1111/J.1365-246X.1967.TB02303.X.

[17] M. Caputo and M. Fabrizio, "A new definition of fractional derivative without singular kernel," *Prog. Fract. Differ. Appl.*, vol. 1, no. 2, Apr. 2015. Accessed: Jan. 1, 2022. [Online]. Available: https://dc.naturalspublishing.com/pfda/vol1/iss2/1

[18] A. Atangana and D. Baleanu, "New fractional derivatives with nonlocal and non-singular kernel: Theory and application to heat transfer model," *Thermal Sci.*, vol. 20, no. 2, pp. 763–769, 2016.

[19] S. Murtaza, M. Iftekhar, F. Ali, Aamina, and I. Khan, "Exact analysis of non-linear electro-osmotic flow of generalized Maxwell nanofluid: Applications in concrete based nano-materials," *IEEE Access*, vol. 8, pp. 96738–96747, 2020, doi: 10.1109/ACCESS.2020.2988259.

[20] S. Murtaza, F. Ali, Aamina, N. A. Sheikh, I. Khan, and K. S. Nisar, "Exact analysis of non-linear fractionalized Jeffrey fluid. A novel approach of Atangana–Baleanu fractional model," *Comput., Mater. Continua*, vol. 65, no. 3, pp. 2033–2047, 2020, doi: 10.32604/CMC.2020.011817.

[21] A. Atangana, "Fractal-fractional differentiation and integration: Connecting fractal calculus and fractional calculus to predict complex system," *Chaos, Solitons Fractals*, vol. 102, pp. 396–406, Sep. 2017, doi: 10.1016/J.CHAOS.2017.04.027.

[22] M. Arfan, H. Alrabaiah, M. U. Rahman, Y.-L. Sun, A. S. Hashim, B. A. Pansera, A. Ahmadian, and S. Salahshour, "Investigation of fractal-fractional order model of COVID-19 in Pakistan under Atangana–Baleanu Caputo (ABC) derivative," *Results Phys.*, vol. 24, May 2021, Art. no. 104046, doi: 10.1016/J.RINP.2021.104046.

[23] Z. Ali, F. Rabiei, K. Shah, and T. Khodadadi, "Qualitative analysis of fractal-fractional order COVID-19 mathematical model with case study of Wuhan," *Alexandria Eng. J.*, vol. 60, no. 1, pp. 477–489, Feb. 2021, doi: 10.1016/J.AEJ.2020.09.020.

[24] Z. Ahmad, F. Ali, N. Khan, and I. Khan, "Dynamics of fractal-fractional model of a new chaotic system of integrated circuit with Mittag-Leffler kernel," *Chaos, Solitons Fractals*, vol. 153, Dec. 2021, Art. no. 111602, doi: 10.1016/J.CHAOS.2021.111602.

[25] A. Rayal and S. R. Verma, "Numerical analysis of pantograph differential equation of the stretched type associated with fractal-fractional derivatives via fractional order Legendre wavelets," *Chaos, Solitons Fractals*, vol. 139, Oct. 2020, Art. no. 110076, doi: 10.1016/J.CHAOS.2020.110076.

[26] Z. Li, Z. Liu, and M. A. Khan, "Fractional investigation of bank data with fractal-fractional caputo derivative," *Chaos, Solitons Fractals*, vol. 131, Feb. 2020, Art. no. 109528, doi: 10.1016/J.CHAOS.2019.109528.

[27] A. Atangana, A. Akgül, and K. M. Owolabi, "Analysis of fractal fractional differential equations," *Alexandria Eng. J.*, vol. 59, no. 3, pp. 1117–1134, Jun. 2020, doi: 10.1016/J.AEJ.2020.01.005.

[28] E. Jimenez, J. Escandón, F. Méndez, and O. Bautista, "Combined viscoelectric and steric effects on the electroosmotic flow in nano/microchannels with heterogeneous zeta potentials," *Colloids Surf. A, Physicochem. Eng. Aspects*, vol. 577, pp. 347–359, Sep. 2019, doi: 10.1016/J.COLSURFA.2019.05.050.

[29] C. Zhao and C. Yang, "Electro-osmotic mobility of non-newtonian fluids," *Biomicrofluidics*, vol. 5, no. 1, Mar. 2011, Art. no. 014110, doi: 10.1063/1.3571278.

[30] S. Ahmed and H. Xu, "Forced convection with unsteady pulsating flow of a hybrid nanofluid in a microchannel in the presence of EDL, magnetic and thermal radiation effects," *Int. Commun. Heat Mass Transf.*, vol. 120, Jan. 2021, Art. no. 105042, doi: 10.1016/J.ICHEATMASSTRANSFER.2020.105042.

[31] A. Abbasi, F. Mabood, W. Farooq, and S. U. Khan, "Radiation and Joule heating effects on electroosmosis-modulated peristaltic flow of Prandtl nanofluid via tapered channel," *Int. Commun. Heat Mass Transf.*, vol. 123, Apr. 2021, Art. no. 105183, doi: 10.1016/J.ICHEATMASSTRANSFER.2021.105183.

[32] D. Mark, S. Haeberle, G. Roth, F. Von Stetten, and R. Zengerle, "Microfluidic lab-on-a-chip platforms: Requirements, characteristics and applications," *NATO Sci. Peace Secur. A Chem. Biol.*, pp. 361–372, 2010, doi: 10.1007/978-90-481-9029-4_17.

[33] Y. Temiz, R. D. Lovchik, G. V. Kaigala, and E. Delamarche, "Lab-on-a-chip devices: How to close and plug the lab?" *Microelectron. Eng.*, vol. 132, pp. 156–175, Jan. 2015, doi: 10.1016/J.MEE.2014.10.013.

[34] A. Banerjee and A. K. Nayak, "Influence of varying zeta potential on non-newtonian flow mixing in a wavy patterned microchannel," *J. Non-Newtonian Fluid Mech.*, vol. 269, pp. 17–27, Jul. 2019, doi: 10.1016/J.JNNFM.2019.05.007.

[35] M. Nazari, S. Rashidi, and J. A. Esfahani, "Mixing process and mass transfer in a novel design of induced-charge electrokinetic micromixer with a conductive mixing-chamber," *Int. Commun. Heat Mass Transf.*, vol. 108, Nov. 2019, Art. no. 104293, doi: 10.1016/J.ICHEATMASSTRANSFER.2019.104293.

[36] B. J. Kirby, "Micro- and nanoscale fluid mechanics: Transport in microfluidic devices," *Brian*, pp. 1–11, 2010. Accessed: Jan. 1, 2022. [Online]. Available: http://books.google.com/books?id=y7PB9f5zmU4C&pgis=1

[37] J. Lyklema and J. T. G. Overbeek, "Electrochemistry of silver iodide the capacity of the double layer at the silver iodide-water interface," *J. Colloid Sci.*, vol. 16, no. 6, pp. 595–608, Dec. 1961, doi: 10.1016/0095-8522(61)90046-0.

[38] J. Marroquin-Desentis, F. Méndez, and O. Bautista, "Viscoelectric effect on electroosmotic flow in a cylindrical microcapillary," *Fluid Dyn. Res.*, vol. 48, no. 3, Apr. 2016, Art. no. 035503, doi: 10.1088/0169-5983/48/3/035503.
[39] E. Jimenez, J. Escandón, F. Méndez, and O. Bautista, "Combined viscoelectric and steric effects on the electroosmotic flow in a microchannel under induced high zeta potentials," *Colloids Surf. A, Physicochem. Eng. Aspects*, vol. 531, pp. 221–233, Oct. 2017, doi: 10.1016/J.COLSURFA.2017.04.081.
[40] L. Cao, P. Zhang, B. Li, J. Zhu, and X. Si, "Numerical study of rotating electro-osmotic flow of double layers with a layer of fractional second-order fluid in a microchannel," *Appl. Math. Lett.*, vol. 111, Jan. 2021, Art. no. 106633, doi: 10.1016/J.AML.2020.106633.
[41] R. D. Baños, J. C. Arcos, O. Bautista, F. Méndez, and E. A. Merchán-Cruz, "Mass transport by an oscillatory electroosmotic flow of power-law fluids in hydrophobic slit microchannels," *J. Brazilian Soc. Mech. Sci. Eng.*, vol. 43, no. 1, pp. 1–15, Jan. 2021, doi: 10.1007/S40430-020-02746-Z.
[42] S. Ghorbani, A. J. Moghadam, A. Emamian, R. Ellahi, and S. M. Sait, "Numerical simulation of the electroosmotic flow of the Carreau-Yasuda model in the rectangular microchannel," *Int. J. Numer. Methods Heat Fluid Flow*, vol. 2021, pp. 1–11, Sep. 2021, doi: 10.1108/HFF-07-2021-0495.
[43] F. Gul, K. Maqbool, and A. B. Mann, "Thermal analysis of electroosmotic flow in a vertical ciliated tube with viscous dissipation and heat source effects," *J. Thermal Anal. Calorimetry*, vol. 143, no. 3, pp. 2111–2123, May 2020, doi: 10.1007/S10973-020-09702-Y.
[44] M. Patel, S. S. H. Kruthiventi, and P. Kaushik, "Polyelectrolyte layer grafting effect on the rotational electroosmotic flow of viscoplastic material," *Microfluid. Nanofluidics*, vol. 25, no. 2, pp. 1–20, Feb. 2021, doi: 10.1007/s10404-020-02412-9.
[45] M. Atlas, S. Hussain, and M. Sagheer, "Entropy generation and unsteady Casson fluid flow squeezing between two parallel plates subject to cattaneo-christov heat and mass flux," *Eur. Phys. J. Plus*, vol. 134, no. 1, p. 33, Jan. 2019, doi: 10.1140/EPJP/I2019-12389-4.
[46] S. A. Shehzad, T. Hayat, and A. Alsaedi, "MHD flow of a Casson fluid with power law heat flux and heat source," *Comput. Appl. Math.*, vol. 37, no. 3, pp. 2932–2942, Jul. 2018, doi: 10.1007/S40314-017-0492-3/TABLES/3.
[47] J. Mackolil and B. Mahanthesh, "Exact and statistical computations of radiated flow of nano and Casson fluids under heat and mass flux conditions," *J. Comput. Design Eng.*, vol. 6, no. 4, pp. 593–605, Oct. 2019, doi: 10.1016/J.JCDE.2019.03.003.
[48] M. Madhu, B. Mahanthesh, N. S. Shashikumar, S. A. Shehzad, S. U. Khan, and B. J. Gireesha, "Performance of second law in carreau fluid flow by an inclined microchannel with radiative heated convective condition," *Int. Commun. Heat Mass Transf.*, vol. 117, Oct. 2020, Art. no. 104761, doi: 10.1016/J.ICHEATMASSTRANSFER.2020.104761.
[49] M. Shruthy and B. Mahanthesh, "Rayleigh-Bénard convection in Casson and hybrid nanofluids: An analytical investigation," *J. Nanofluids*, vol. 8, no. 1, pp. 222–229, Jan. 2019, doi: 10.1166/JON.2019.1571.
[50] B. Mahanthesh, B. J. Gireesha, M. Sheikholeslami, S. A. Shehzad, and P. B. S. Kumar, "Nonlinear radiative flow of Casson nanoliquid past a cone and wedge with magnetic dipole: Mathematical model of renewable energy," *J. Nanofluids*, vol. 7, no. 6, pp. 1089–1100, Dec. 2018, doi: 10.1166/JON.2018.1546.
[51] J. Mackolil and B. Mahanthesh, "Sensitivity analysis of radiative heat transfer in Casson and nano fluids under diffusion-thermo and heat absorption effects," *Eur. Phys. J. Plus*, vol. 134, no. 12, p. 619, Dec. 2019, doi: 10.1140/EPJP/I2019-12949-6.
[52] B. Mahanthesh and B. J. Gireesha, "Thermal Marangoni convection in two-phase flow of dusty Casson fluid," *Results Phys.*, vol. 8, pp. 537–544, Mar. 2018, doi: 10.1016/J.RINP.2017.12.066.
[53] J. Escandón, E. Jiménez, C. Hernández, O. Bautista, and F. Méndez, "Transient electroosmotic flow of Maxwell fluids in a slit microchannel with asymmetric zeta potentials," *Eur. J. Mech. B/Fluids*, vol. 53, pp. 180–189, Sep. 2015, doi: 10.1016/J.EUROMECHFLU.2015.05.001.
[54] N. A. Sheikh, D. L. C. Ching, T. Abdeljawad, I. Khan, M. Jamil, and K. S. Nisar, "A fractal-fractional model for the MHD flow of casson fluid in a channel," *Comput., Mater. Continua*, vol. 67, no. 2, pp. 1385–1398, 2021.
[55] N. Khan, F. Ali, M. Arif, Z. Ahmad, A. Aamina, and I. Khan, "Maxwell nanofluid flow over an infinite vertical plate with ramped and isothermal wall temperature and concentration," *Math. Problems Eng.*, vol. 2021, pp. 1–19, Sep. 2021, doi: 10.1155/2021/3536773.

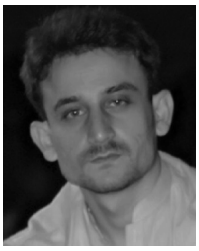

SAQIB MURTAZA is currently pursuing the Ph.D. degree in mathematics with the King Mongkut's University of Technology Thonburi, Thailand. He is doing his research work under the supervision of Professor Dr. Poom Kumam. He has published six research articles in different well-reputed high-impact factor international journals of the world. His most experience has been working in the academic sector and has expertise in the area of fluid dynamics, MHD flows, nanofluids, fractional derivatives, integral transforms, exact solutions, numerical solutions, and mathematical modeling.

POOM KUMAM (Member, IEEE) received the Ph.D. degree in mathematics from Naresuan University, Thailand. He is currently a Full Professor with the Department of Mathematics, King Mongkut's University of Technology Thonburi (KMUTT), where he is also the Head of the Fixed Point Theory and Applications Research Group. He is also with the Theoretical and Computational Science Center (TaCS-Center), KMUTT, and the Director of the Computational and Applied Science for Smart Innovation Cluster (CLASSIC Research Cluster), KMUTT. He has authored or coauthored more than 800 international peer-reviewed journals. His main research interests include fixed point theory and applications, computational fixed point algorithms, nonlinear optimization, control theory, and optimization algorithms.

ZUBAIR AHMAD received the B.S. degree in mathematics from the University of Peshawar and the M.S. degree in mathematics from the City University of Science and Information Technology, Peshawar, Pakistan. He is currently pursuing the Ph.D. degree in applied mathematics with the Department of Mathematics and Physics, University of Campania, Caserta, Italy. He has published seven research articles in different well-reputed high-impact factor international journals of the world. His research interests include heat and mass transfer, fluid dynamics, mathematical epidemiology, modeling of infectious diseases, chaos theory, dynamical systems, chemical kinetics, reaction dynamics, modeling of biochemical reactions, and mathematical psychology, such as love affair models, stability analysis, fractional and fractal derivatives, numerical, analytical, and exact solutions.

KANOKWAN SITTHITHAKERNGKIET received the B.Sc., M.Sc., and Ph.D. degrees. She is currently a Associate Professor with the Department of Mathematics, King Mongkut's University of Technology North Bangkok (KMUTNB). Her research interests include optimization, nonlinear mappings, least squares method, optimization problems, image processing, fractional and fractal derivatives, numerical, analytical, and exact solutions.

IBN E ALI is currently pursuing the B.S. degree in mathematics with the Government Superior Science College Peshawar, University of Peshawar, Pakistan. His most expertise is in the area of fluid dynamics, MHD flows, nanofluids, fractional derivatives, integral transforms, exact solutions, numerical solutions, and mathematical modeling.